

The velocity dispersion profile of globular clusters : a closer look

François Roueff¹, Pierre Salati^{1,2}, and Richard Taillet³

¹ Laboratoire de Physique Théorique ENSLAPP, BP110, F-74941 Annecy-le-Vieux Cedex, France.

² Université de Savoie, BP1104 73011 Chambéry Cedex, France.

³ The Center for Particle Astrophysics, Le Conte Hall, University of California at Berkeley, Berkeley, CA, 94720, USA.

Received / Accepted

Abstract. Measurements of the surface brightness distribution and of the velocity dispersion profile have been so far used to infer the inner dynamics of globular clusters. We show that those observations do not trace back the dark matter potentially concealed in these systems in the form of low-mass compact objects. We have built Michie models of globular clusters which contain both massive and low-mass stars. An analytic expression for the stellar mass densities has been explicitly derived in terms of the usual error function and Dawson's integral. While the heavy population is kept fixed, the abundance of the light species of our models is varied. When stellar velocities are anisotropic, both the surface brightness and the velocity dispersion profiles of the cluster become insensitive to the abundance of low-mass stars. This suggests that the actual stellar mass function of many globular clusters is still to be discovered.

1. Introduction

Among the different kinds of astrophysical star conglomerates, globular clusters (GC) have a very peculiar status. First, as we go down the mass-scale of observed structures, from super clusters through galaxies down to dwarf spheroidals, they are the first objects whose dynamics can be understood without resorting to the presence of dark matter. Second, and this may be related to the first point, they are the only star clusters dense enough for a statistical equilibrium to be reached in a Hubble timescale. The dark matter content of globular clusters may be an important clue to the understanding of the formation of our galaxy. However, the observational situation is not very clear yet as regards stellar counts and the related direct detection of a hidden population of light and faint stars. Since the claim by Richer and Fahlman that the mass function steeply rises towards low masses in some

GCs (Fahlman et al. 1989, Richer et al. 1991), the Hubble Space Telescope (HST) has been used to measure the mass function in several globular clusters, and the opposite conclusion was reached (Demarchi and Paresce 1995, Elson et al. 1995, Paresce, De Marchi and Romaniello 1995). Part of the discrepancy is due to the conversion scheme used to translate the measured luminosity functions into mass functions. There is actually no consensus on the mass-to-luminosity relation of low-mass objects. In a recent investigation, Santiago et al. (1996) found a steadily increasing mass function for ω Cen, using HST observations. This suggests that the dark matter content may depend on the cluster. It seems therefore important to fully understand what we can also learn from other types of measurement, such as in particular the brightness and the velocity dispersion profiles.

There is a widespread belief that globular clusters cannot contain large amounts of dark matter, because of the Virial theorem. The latter relates the velocity dispersion σ at the center of the cluster to the total mass M_t and to the half-mass radius r_h of the system. For a one-component globular cluster, that relation may be expressed as (Spitzer 1987) :

$$\langle \sigma^2 \rangle \approx 0.4 \frac{GM_t}{r_h} \quad (1)$$

However, if a dark component is also present, in the form of low-mass objects for example, the virial theorem must be modified to

$$\sum_i M_t(i) \langle \sigma^2 \rangle_i = E_p, \quad (2)$$

where the index i refers to the different stellar species, and where E_p is the potential energy of the cluster. In previous papers (Taillet et al. 1995 and 1996) focusing on isotropic globular clusters, we showed that in the presence of dark matter, relation (1) still holds for the visible component, and that most of the visible properties of the cluster are approximately the same as for a one-component system. In particular, the brightness profile is nearly unchanged even if dark matter is abundant. This is due to the phenomenon of mass segregation. Because of gravitational interactions,

Send offprint requests to: Pierre Salati

Correspondence to: Pierre Salati

stars tend to share their kinetic energy. Thus, the light objects gain velocity from the heavier stars, which sink to the center of the cluster, while the light objects have a much more diffuse distribution. The heavier stars then form a self-gravitating system in the low-density background of the light objects, and their properties are not significantly altered. It was concluded that even a dark-matter dominated cluster looks very much the same as a dark-matter free system, and that the point of the dark matter content could not be made by the mere observation of the brightness profile.

It was also noted that the presence of dark matter would be betrayed by the velocity dispersion profile of bright stars which flattens when dark matter is present. However, those profiles need to be accurately measured, which is not yet the case. The results of our analysis were obtained for King models where the stellar distribution is isotropic in velocity space. Their validity must be reassessed when the velocity distribution is no longer isotropic. Anisotropy is likely to be present at some level because stars mainly interact in the cluster core. At least part of those orbiting at the outskirts of the system gained the required energy by interacting at the center. Then, orbits should be predominantly radial at large radii. In that respect, note that ωCen for which the HST observations provide a steadily rising mass function may also have an anisotropic velocity distribution (Meylan 1987), even though an isotropic distribution is not excluded (Merrit et al. 1996). Such a cluster may be modeled by a Michie distribution in phase space, where an angular-momentum exponential cut-off is applied to a King distribution (see section 2).

It is well known that when anisotropy is present, the velocity dispersion profile is less flat. Thus we suspect that the flattening of the velocity dispersion profile that occurs in the presence of dark matter will be partially cancelled by the effect of anisotropy. A given velocity dispersion profile could therefore be interpreted either with a one-component isotropic GC or with a two-component anisotropic GC. However, anisotropy may also affect a priori the brightness profile. The main goal of this paper is therefore to make these statements more quantitative. We will investigate how anisotropy affects the detectability of dark matter in globular clusters. In section 2, we present a new analytic form for the equation that relates the gravitational potential to the stellar mass densities. The Michie distribution is expressed with the usual error function and Dawson's integral. Section 3 is devoted to our set of two-component Michie models whose heavy component is kept fixed while the abundance in low-mass stars is varied. Various velocity anisotropies are explored. Finally, the surface brightness and the velocity dispersion profiles of these models are discussed in section 4 and conclusions are drawn.

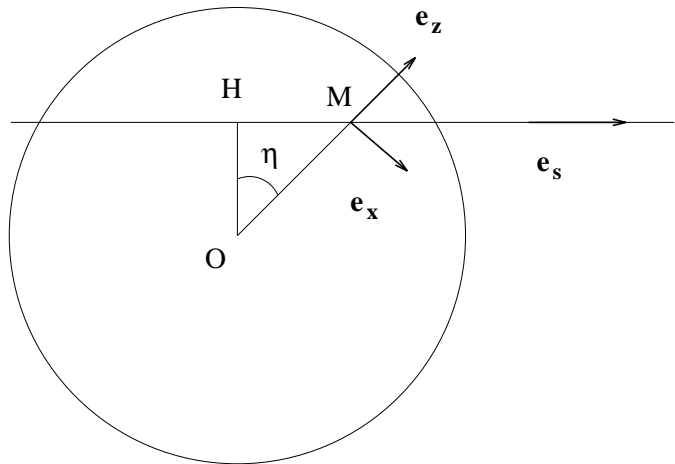


Fig. 1. The unit vector \mathbf{e}_s is aligned along the line of sight HM that crosses the globular cluster. At the pericenter H, the distance to the center O is minimal. At any given point M on the line of sight, with position labelled by the angle η , a convenient frame may be defined as presented here.

2. The Michie distribution functions

A Michie model of a globular cluster is spherically symmetric as regards its distribution of stars in space. However, its velocity ellipsoid tends to be elongated towards the center of the cluster for radii larger than some critical value r_a . The phase space distribution of a stellar species with mass m and whose one-dimensional velocity dispersion is σ , may be expressed as

$$f(r, \mathbf{v}) = k e^{-L^2/2r_a^2\sigma^2} \left\{ e^{\mathcal{E}/\sigma^2} - 1 \right\}, \quad (3)$$

where $\mathbf{L} = \mathbf{OM} \wedge \mathbf{v}$ is the orbital momentum of the stars located at point M and whose velocities are \mathbf{v} . That orbital momentum is defined with respect to the cluster center O. The quantity \mathcal{E} is related to the stellar energy per unit mass $E = \Phi(r) + v^2/2$ through

$$\mathcal{E} = \Phi_t - E, \quad (4)$$

where $\Phi_t = \Phi(r_t)$ is the gravitational potential at the tidal boundary r_t of the cluster. Whenever \mathcal{E} is negative, the distribution function f vanishes. Inside the radius of anisotropy r_a , the distribution of stellar velocities is spherical. Beyond r_a , it straightens in the direction of the cluster center. At remote distances, trajectories are almost radial. This is a major difference with King models for which velocities are spherically distributed. The mass density is now given by a double integral. The orbital momentum $L = r v \sin \theta$ depends actually on both the magnitude v of the velocity and on the angle θ between the latter and the radial direction \mathbf{OM} . Defining the variables $x = v/\sqrt{2}\sigma$ and $y = \cos \theta$ yields a mass density

$$\rho(r) = 4\pi k m (2\sigma^2)^{3/2} \mathcal{H}(u, \alpha) \quad (5)$$

proportional to the double integral

$$\mathcal{H}(u, \alpha) = \int_0^1 dy \int_0^{\sqrt{u}} dx x^2 h(x, y), \quad (6)$$

where the function $h(x, y)$ is defined as

$$h(x, y) = e^{-\alpha^2 x^2 (1 - y^2)} \left\{ e^{(u - x^2)} - 1 \right\} . \quad (7)$$

The parameter $u = (\chi - \psi)$ is the difference between the reduced potential $\chi = \Phi_t/\sigma^2$ at the tidal boundary r_t of the system and its counterpart $\psi = \Phi(r)/\sigma^2$ at distance r from the cluster center. The ratio r/r_a is denoted by α . The scaling factor between the mass density $\rho(r)$ and the integral (6) may also be inferred from the relation

$$\frac{\rho(r)}{\rho(0)} = \frac{\mathcal{H}(u, \alpha)}{\mathcal{H}(\chi, 0)} , \quad (8)$$

where $\rho(0)$ denotes the stellar mass density at the cluster center.

So far, expression (6) was estimated numerically through a direct integration. We have derived here an analytic development of $\mathcal{H}(u, \alpha)$ in terms of the functions

$$d(x) = e^{-x^2} \int_0^x e^{t^2} dt \quad (9)$$

and

$$e(x) = e^{x^2} \int_0^x e^{-t^2} dt . \quad (10)$$

The first integral is called the Dawson's function and may be easily computed thanks to a convenient approximation due to Rybicki (Rybicki 1989 and Numerical Recipes). The function $e(x)$ is related to the error function

$$e(x) = \frac{\sqrt{\pi}}{2} e^{x^2} \operatorname{erf}(x) . \quad (11)$$

The distribution function $f(r, \mathbf{v})$ can be averaged over the angle θ to yield a King distribution up to a correction factor

$$f(r, v) = k \left\{ e^{\mathcal{E}/\sigma^2} - 1 \right\} \left\{ \frac{d(\alpha x)}{\alpha x} \right\} . \quad (12)$$

The parameter αx stands for the ratio $rv/\sqrt{2}r_a\sigma$. Inside the radius of anisotropy, αx is small compared to unity and the correction factor $d(\alpha x)/\alpha x$ of relation (12) reduces to 1. A King distribution is therefore recovered when the radius r is smaller than r_a . After an integration on the magnitude v of the velocity, relation (6) may be expressed as

$$\mathcal{H}(u, \alpha) = \frac{1}{2(1 + \alpha^2)} \left[e(\sqrt{u}) - \sqrt{u} + \frac{d(\alpha\sqrt{u}) - \alpha\sqrt{u}}{\alpha^3} \right] \quad (13)$$

Several approximations to that expression are given in the Appendix depending on whether \sqrt{u} and $\alpha\sqrt{u}$ are large or not with respect to unity.

The dispersion velocity profile of globular clusters may be defined in various ways. What astronomers actually measure is the velocity of some stellar species along the line of sight. Suppose that a specific pixel contains N stars with same spectral type. The radial velocity of the i^{th} object of the sample is denoted by v_i . A variety of statistical averages can be performed, each yielding a different value

for the dispersion. In this article, the dispersion velocity \bar{v}_{rad} along the line of sight will be defined as

$$\bar{v}_{\text{rad}} = \left\{ \sum_{i=1}^N \frac{v_i^2}{N} \right\}^{1/2} . \quad (14)$$

In our two component models, we will be interested in the velocity dispersion profile of the heavy and bright stellar population for which spectral measurements can be performed.

Let us consider now a line of sight with direction set by the unit vector \mathbf{e}_s as shown in Fig. 1. At the pericenter H, the distance to the center O is minimal. For any given point M along that line of sight, a convenient frame may be defined with its unit vector \mathbf{e}_z pointing outwards in the same direction as the vector \mathbf{OM} . The unit vector \mathbf{e}_x is perpendicular to \mathbf{e}_z and is in the plane defined by the three points O, H and M. Finally, the last basis vector \mathbf{e}_y is defined as the product $\mathbf{e}_z \wedge \mathbf{e}_x$. The position of point M may be traced by the angle η between the vectors \mathbf{OH} and \mathbf{OM} . The projection v_s of the velocity along the line of sight is then given by

$$\mathbf{e}_s \cdot \mathbf{v} = v_x \cos \eta + v_z \sin \eta . \quad (15)$$

Its square v_s^2 may be averaged locally to yield

$$\langle v_s^2 \rangle = \langle v_x^2 \rangle \cos^2 \eta + \langle v_z^2 \rangle \sin^2 \eta . \quad (16)$$

Because the velocity distribution is axisymmetric around the direction connecting point M to the cluster center O, the contribution of the product $v_x v_z$ to the local average of the line of sight velocity v_s^2 vanishes. The latter may be expressed in terms of the functions $\mathcal{I}(u, \alpha)$ and $\mathcal{J}(u, \alpha)$

$$\rho(M) \left\langle \left(\frac{v_s}{\sigma} \right)^2 \right\rangle = 4\pi k m (2\sigma^2)^{3/2} \{ \mathcal{I} + \mathcal{J} \sin^2 \eta \} \quad (17)$$

where $\rho(M)$ denotes the mass density of the stellar species with mass m under consideration at the point M . The functions \mathcal{I} and \mathcal{J} are respectively defined by the integrals

$$\mathcal{I}(u, \alpha) = \int_0^1 dy \int_0^{\sqrt{u}} dx x^4 (1 - y^2) h(x, y) , \quad (18)$$

and

$$\mathcal{J}(u, \alpha) = \int_0^1 dy \int_0^{\sqrt{u}} dx x^4 (3y^2 - 1) h(x, y) . \quad (19)$$

The functions \mathcal{H} and \mathcal{I} are related by

$$\mathcal{I}(u, \alpha) = - \frac{\partial \mathcal{H}}{\partial \alpha^2} , \quad (20)$$

so that \mathcal{I} may be expressed as

$$\begin{aligned} (1 + \alpha^2) \mathcal{I}(u, \alpha) &= \mathcal{H} + \frac{3}{4\alpha^5} \{ d(\alpha\sqrt{u}) - \alpha\sqrt{u} \} \\ &\quad + \frac{u}{2\alpha^3} d(\alpha\sqrt{u}) . \end{aligned} \quad (21)$$

The calculation of the function \mathcal{J} is slightly more involved and yields

$$\begin{aligned} (1 + \alpha^2)^2 \mathcal{J}(u, \alpha) &= \frac{\alpha^2}{2} \{ e(\sqrt{u}) - \sqrt{u} \} \\ &\quad + (\alpha^2 + u + u\alpha^2) \frac{u^{3/2}}{3} \\ &\quad - \mathcal{K}(u, \alpha) \{ d(\alpha\sqrt{u}) - \alpha\sqrt{u} \} , \end{aligned} \quad (22)$$

where

$$\mathcal{K}(u, \alpha) = \frac{2\alpha^2 + (1 + \alpha^2)(5 + 2u\alpha^2)}{4\alpha^5} . \quad (23)$$

Notice that v_s^2 needs eventually to be averaged along the entire line of sight. The end result is therefore the radial average

$$\bar{v}_{\text{rad}}^2 = \frac{\int \rho(M) \langle v_s^2 \rangle ds}{\int \rho(M) ds} , \quad (24)$$

to be compared with the observational definition (14).

3. The models

To test the sensitivity of observable quantities to the amount of dark matter, we built two-component Michie models of globular clusters, with both a heavy and a light stellar population. One of the components encapsulates the visible, solar mass stars while the other component is dark matter in the form of low-mass objects with mass $m_2 = 0.1 M_\odot$. The indexes 1 and 2 respectively refer to the bright and dark populations. We built 25 globular clusters, with anisotropy radii $z_a = 1000, 100, 50, 20$ and 10 , and dark matter content $M_2/M_1 = 0, 1, 3, 6$ and 10 . The parameter z_a stands for the ratio of the anisotropy radius r_a to the typical scale length a yet to be defined. Models with $z_a = 1000$ may be considered as King models. In that case, the anisotropy radius is so large that it contains most of the cluster, hence a spherical velocity distribution almost everywhere. A two-component Michie model is completely specified by six parameters, namely the anisotropy radius r_a , the velocity dispersions σ_1 and σ_2 of the two species, the normalization factors k_1 and k_2 (or alternatively the central densities ρ_{c1} and ρ_{c2}), and finally the depth of the gravitational potential well $\chi = \Phi_t/\sigma_1^2$. These parameters are entirely determined by the following conditions :

- (i) The velocity dispersion for the luminous stars is measured. We will adopt the typical value $\sigma_1 = 7$ km/s.
- (ii) The two species are in thermal equilibrium, imposing the relation $m_1\sigma_1^2 = m_2\sigma_2^2$ which sets σ_2 equal to $\sqrt{10} \times \sigma_1$.
- (iii) The visible central density is set to $\rho_{c1} = 8000 M_\odot/\text{pc}^3$. This leads to models having almost the same central brightness which, as a matter of fact, is a well measured quantity.
- (iv) The anisotropy radius has been varied as explained above. The smaller r_a , the stronger the anisotropy.
- (v) The total visible luminosity is also a well determined quantity. Here, it has been set equal to a typical value $L_1 = 3 \times 10^5 L_\odot$. Throughout our set of models, ρ_{c2} and χ have been chosen to yield that total luminosity, as well as the above mentioned ratios M_2/M_1 .

Remember that M_1 and M_2 respectively stand for the total mass in heavy and in low mass stars. Visible stars

are assumed to have a standard solar L/M ratio. Low mass objects are too faint to shine and their luminosity is negligible.

The structure of the cluster is determined by the Poisson equation where the local mass density is given by

$$\rho(r) = \rho_{c1} \frac{\mathcal{H}(u, \alpha)}{\mathcal{H}(\chi, 0)} + \rho_{c2} \frac{\mathcal{H}(m_2 u/m_1, \alpha)}{\mathcal{H}(m_2 \chi/m_1, 0)} . \quad (25)$$

Introducing the dimensionless radius $z = r/a$ where the typical scale length a is defined as

$$a = \frac{\sigma_1}{\sqrt{4\pi G \rho_{c1}}} , \quad (26)$$

leads to the differential equation

$$\frac{1}{z^2} \frac{d}{dz} \left(z^2 \frac{du}{dz} \right) = - \frac{\mathcal{H}(u, \alpha)}{\mathcal{H}(\chi, 0)} - \left(\frac{\rho_{c2}}{\rho_{c1}} \right) \frac{\mathcal{H}(m_2 u/m_1, \alpha)}{\mathcal{H}(m_2 \chi/m_1, 0)}$$

Once that equation is solved and the structure of the cluster is determined, the velocity dispersion and the surface brightness profiles are computed. The former is evaluated with the help of relation (24). The latter is just the surface mass density of heavy stars

$$\Sigma_1 = \int \rho_1(m) ds , \quad (27)$$

up to the factor $(L_\odot/M_\odot)/4\pi$.

4. Discussion and conclusions

Profiles of the surface mass density Σ_1 and of the velocity dispersion \bar{v}_{rad} for the heavy component of our models are presented in Fig. 2 and 3 respectively. Low mass stars do not shine in the V band and therefore do not contribute to the surface luminosity of the cluster. Figure 2 shows that whatever the anisotropy radius z_a , the brightness profiles are almost not affected by the dark matter content of the cluster. At constant z_a , the various curves are superimposed while the light to heavy component mass ratio M_2/M_1 increases from 0 to 10. This result was already obtained in the case of King models (Taillet et al. 1995 and 1996) and its validity is now extended to Michie clusters. For $z_a = 10$ and 20 , the surface luminosity drops like $r^{-5/2}$ as expected for a strongly anisotropic system. In Fig. 3, the velocity dispersion profiles are presented. For $z_a = 1000$, velocities are almost spherically distributed and the curves are different when the dark matter abundance M_2/M_1 varies. However, the velocity dispersion along the line of sight becomes insensitive to the dark matter content of the cluster when the anisotropy of the velocity distribution increases. For z_a smaller than 20 , the various profiles start to be fairly similar and become hard to disentangle observationally. Beyond the radius of anisotropy r_a , the stellar orbital velocity $v_\theta = v \sin \theta$ is dominated on average by the Michie exponential cut-off on the orbital momentum. The orbital velocity is in that case of order $v_\theta \sim \sigma r_a/r$. It is no longer sensitive to the gravitational potential. The velocity dispersion \bar{v}_{rad} measured

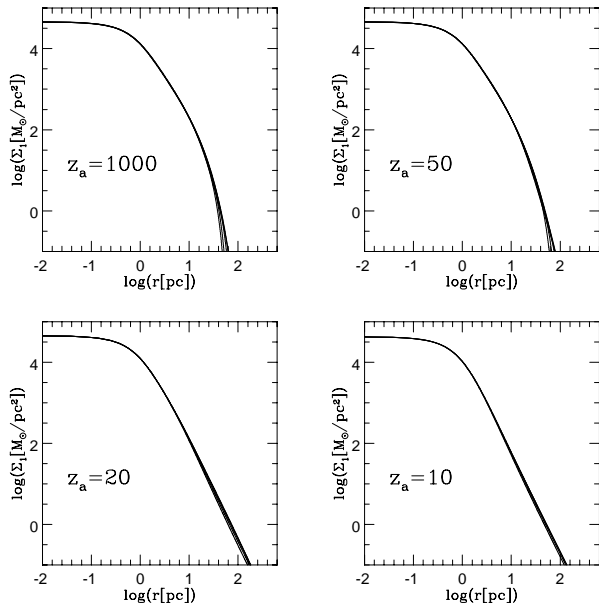


Fig. 2. In each of the four plots, the surface mass density Σ_1 of the heavy population of our models is presented as a function of the radius r . The mass ratio M_2/M_1 is set equal to the five different values 0, 1, 3, 6 and 10. The radius of anisotropy z_a decreases from 1000, where a King model is recovered with a spherical distribution of velocity, down to 10 for which the anisotropy is strong and the stellar orbits almost radial. In each plot, the curves are hard to disentangle. The surface brightness profile is insensitive to the dark matter content M_2 of the cluster.

along the line of sight, to which the orbital velocity contributes most, is therefore blind to the mass content of the cluster. As z_a decreases, the effect is more and more pronounced. When it becomes dominant everywhere outside the core radius of the cluster, the gravitational potential and therefore the dark matter of the system have little effect on \bar{v}_{rad} , hence the degeneracy of the profiles in Fig. 3 for $z_a = 10$. Note that as velocities become radially distributed, light stars need more space to contribute the same dark mass as a result of the conservation of the phase space volume. At fixed M_2/M_1 ratio, low mass stars extend further away as the velocity anisotropy increases. However, there is still a substantial amount of them inside the visible part of the cluster. When $z_a = 10$ for instance, the dark mass inside the inner 60 pc is respectively 4.7×10^4 , 1.3×10^5 , 2.2×10^5 and $2.9 \times 10^5 M_\odot$ for a light to heavy stellar mass ratio M_2/M_1 of 1, 3, 6 and 10.

The dashed curve that appears in three of the plots of Fig. 3 is the velocity dispersion profile for a King model with no low mass stars. That case is degenerate with the entire set of Michie clusters with $z_a = 20$, whatever their dark matter content. The same velocity dispersion profile may therefore be interpreted either with a one-component

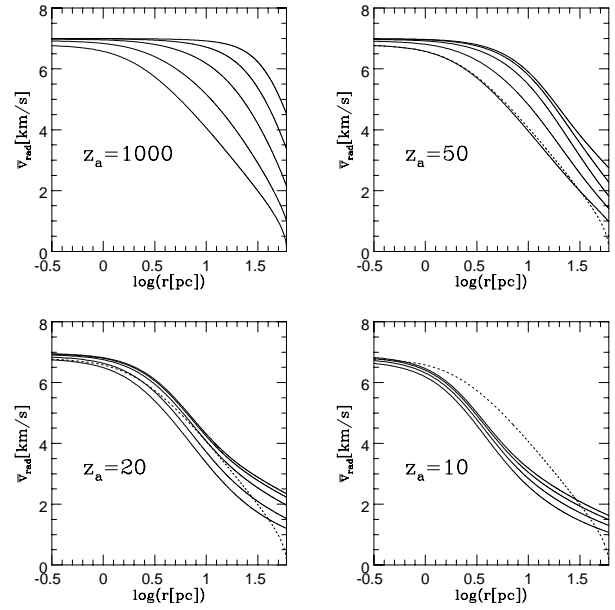


Fig. 3. Same as in figure 2 with the velocity dispersion profiles. For $z_a = 1000$, velocities are almost spherically distributed and the curves are different when the dark matter abundance M_2/M_1 varies. However, the velocity dispersion along the line of sight becomes insensitive to the dark matter content of the system when the anisotropy of the velocity distribution increases. The dashed curve that appears in three of the plots is the velocity dispersion profile for a King model with no low mass stars. That case is degenerate with the entire set of Michie clusters with $z_a = 20$. The same velocity dispersion profile may therefore be interpreted either with a one-component isotropic cluster or, alternatively, with an anisotropic system containing dark matter.

isotropic cluster or, alternatively, with an anisotropic system containing dark matter. If so, the degeneracy may be lifted by the distribution of surface luminosity. Note however that the brightness profiles become different far from the center, in a region where the surface mass density Σ_1 has already dropped by four orders of magnitude with respect to its central value. Figures 2 and 3 illustrate actually the difficulty to estimate the amount of low mass stars potentially concealed in globular clusters from their velocity dispersion profiles and from the distributions of their surface luminosities. Both measurements have been used so far to determine the mass content of GCs. We therefore conclude that the same set of observations may be interpreted by quite different models. This suggests that the actual stellar mass function of many globular clusters needs to be reinvestigated.

Dark matter in globular clusters should be traced by the three dimensional velocity distribution of bright stars. We have just shown that the projection along the line of

sight alone does not lead to a unique answer. Another possibility is the search for tidal tails. If present, dark matter dominates the gravity of the outskirts of clusters and prevents heavy stars from evaporating (Moore 1996). Tidal tails exist whenever dark matter is not present to play that inhibition effect. As mentioned by Taillet et al. (1995 and 1996), the presence of low mass stars should also lead to an infrared halo surrounding the bright central part. Finally, if the cluster lies against a rich stellar background, low mass stars should also induce a few gravitational microlensing events.

Acknowledgements. This work has been carried out under the auspices of the Human Capital and Mobility Programme of the European Economic Community, under contract number CHRX-CT93-0120 (DG 12 COMA).

References

- De Marchi, G., Paresce, F., 1995, A&A 304, 202
 Elson, R.A.W., Gilmore, G., Santiago, G.X., Casertano, S., AJ 110, 682
 Fahlman, G.G., Richer, H.B., Searle, L., Thompson, I.B., 1989, ApJ 343, L49
 Merrit, D., Meylan, G., Mayor, M., 1996, preprint astro-ph/9612184
 Meylan, G., 1987, A&A 184, 144
 Moore, B., 1996, ApJ 461, L13
 Press, W.H, 1995, Numerical Recipes in C : the Art of Scientific Computing, 2nd edition, Cambridge University Press
 Paresce, F., De Marchi, G., Romaniello, M., 1995, ApJ 440, 216
 Richer, H.B., Fahlman, G.G., Buonnano, R., Fusi Pecci, F., Searle, L., Thompson, I.B., 1991, ApJ 381, 147
 Rybicki, G.B., 1989, Computers in Physics 3, 85
 Santiago, B.X., Elson, R.A.W., Gilmore, G.F., MNRAS 281, 1363
 Spitzer, L.Jr, 1987, Dynamical evolution of globular clusters, Princeton University Press
 Taillet, R., Longaretti, P.-Y., Salati, P., 1995, Astroparticle Physics 4, 87
 Taillet, R., Salati, P., Longaretti, P.-Y., 1996, ApJ 461, 104

Appendix A: Useful expansions

The functions $d(x)$ and $e(x)$ may be expanded as power series of the variable x when the latter is small. The Dawson's function is given by

$$d(x) = x - A_1 x^3 + A_1 A_2 x^5 + \dots + (-1)^n A_1 A_2 \dots A_n x^{2n+1} + \dots, \quad (\text{A1})$$

whereas

$$e(x) = x + A_1 x^3 + A_1 A_2 x^5 + \dots + A_1 A_2 \dots A_n x^{2n+1} + \dots. \quad (\text{A2})$$

The constants A_n stand for the ratios $2/(2n+1)$. Whenever $\alpha\sqrt{u}$ or \sqrt{u} are small compared to 1, expansions (A1)

or (A2) should be used in expression (13). If both variables are small at the same time, the expansion becomes

$$\begin{aligned} \mathcal{H}(u, \alpha) = & \frac{u^{5/2}}{2} A_1 A_2 \{ 1 + A_3 u (1 - \alpha^2) \\ & + A_3 A_4 u^2 (1 - \alpha^2 + \alpha^4) \\ & + A_3 A_4 A_5 u^3 (1 - \alpha^2 + \alpha^4 - \alpha^6) \\ & + A_3 A_4 A_5 A_6 u^4 (1 - \alpha^2 + \alpha^4 - \alpha^6 + \alpha^8) \\ & + \dots \} \end{aligned} \quad (\text{A3})$$

In the same limit, the function \mathcal{I} may be expanded as

$$\begin{aligned} \mathcal{I}(u, \alpha) = & \frac{u^{7/2}}{2} A_1 A_2 A_3 \{ 1 + A_4 u (1 - 2\alpha^2) \\ & + A_4 A_5 u^2 (1 - 2\alpha^2 + 3\alpha^4) \\ & + A_4 A_5 A_6 u^3 (1 - 2\alpha^2 + 3\alpha^4 - 4\alpha^6) \\ & + A_4 A_5 A_6 A_7 u^4 (1 - 2\alpha^2 + 3\alpha^4 - 4\alpha^6 + 5\alpha^8) \\ & + \dots \} \end{aligned} \quad (\text{A4})$$

whereas \mathcal{J} is a sum of three series expansions

$$\begin{aligned} (1 + \alpha^2)^2 \mathcal{J}(u, \alpha) = & \frac{u^{9/2}}{15} \alpha^2 A_3 A_4 \{ 2\mathcal{J}_a(u) \\ & - (5 + 7\alpha^2) \alpha^2 \mathcal{J}_b(u\alpha^2) \\ & + 9(1 + \alpha^2) \alpha^2 \mathcal{J}_c(u\alpha^2) \} . \end{aligned} \quad (\text{A5})$$

The functions \mathcal{J}_a , \mathcal{J}_b and \mathcal{J}_c are respectively defined by

$$\mathcal{J}_a(x) = 1 + A_5 x + A_5 A_6 x^2 + A_5 A_6 A_7 x^3 + \dots \quad (\text{A6})$$

$$\mathcal{J}_b(x) = 1 - A_5 x + A_5 A_6 x^2 - A_5 A_6 A_7 x^3 + \dots \quad (\text{A7})$$

while

$$\mathcal{J}_c(x) = 1 - A_4 x \mathcal{J}_b(x) . \quad (\text{A8})$$